



## Development and photocatalytic activities of TiO<sub>2</sub> doped with Ca–Ce–W in the degradation of acid red 1 under visible light irradiation

U.G. Akpan<sup>a,b</sup>, B.H. Hameed<sup>a,\*</sup>

<sup>a</sup>*School of Chemical Engineering, Engineering Campus, Universiti Sains Malaysia, Nibong Tebal, Penang 14300, Malaysia*

*Tel. +604 599 6422; email: chbassim@eng.usm.my*

<sup>b</sup>*Chemical Engineering Department, Federal University of Technology, Minna, Nigeria*

Received 10 January 2012; Accepted 20 May 2013

---

### ABSTRACT

A stable visible light photocatalyst has successfully been developed by doping titanium dioxide (TiO<sub>2</sub>) with Ca, Ce, and W. Various combinations were developed and tested. The photocatalyst, when subjected to visible light photocatalytic degradation of C.I. Acid red 1 (AR1) showed an excellent performance in comparison with the most acclaimed commercial TiO<sub>2</sub> photocatalyst, Degussa P25. The photocatalytic process with the best developed photocatalyst is “initial-concentration”-dependent, as high initial concentrations of AR1 dye precluded the photon energy from reaching the photocatalyst, and hence reduced its degradation rate. Initial pH of dye solution exerts its influence on the visible light photocatalytic degradation of the dye. High initial pH 10 was detrimental to the process, while the process was controlled by adsorption at lower pH 3. The developed photocatalysts were characterized by X-ray photoelectron spectroscopy, UV–vis diffuse reflectance spectra, X-ray diffraction, N<sub>2</sub> physisorption, surface scanning electron microscopy, and fourier transform infra-red spectroscopy. The results showed a red shift in the band gap of the tri-doped TiO<sub>2</sub> from 3.2 to 2.94 eV indicating a shift in the onset optical wavelength from 387.19 to 421.43 nm.

*Keywords:* Photocatalyst; Degradation; Visible light; Optical wavelength; Dye

---

### 1. Introduction

Global industrialization is not without its attendant challenges. The release of unwanted by-products and pollutants into the environment by textiles, chemicals, and processing industries is directly proportional to industrial growth. The effluents from these industries released into the air and water channels are carcinogenic and toxic and must be removed to keep

the environment safe. Dyes of all types and pesticides are usually released as effluents into water channels by textile/food and agro-chemical industries. Much research has been conducted to remove pollutants from wastewaters before discharge into the environment [1–6]. Since most of these pollutants are non-biodegradable and recalcitrant, conventional methods such as adsorption by activated carbon, nanofiltration, ozonation, and biodegradation cannot be the best approach for their removal from wastewaters.

---

\*Corresponding author.

Recent studies [7–14] showed that advanced oxidation processes, particularly, photocatalysis which is aimed at the destruction of the pollutants in wastewaters, is widely used. Many types of semiconductor photocatalysts have also been employed in the degradation of pollutants in wastewaters [15–20]. Among these semiconductor photocatalysts, titanium dioxide ( $\text{TiO}_2$ ) is widely employed because of its merits. It is biochemically inert, photocatalytically stable, relatively easy to produce and use, able to efficiently catalyze reactions, cheap, and without risk to the environment or humans [21].

Despite the advantages surrounding  $\text{TiO}_2$ , its application in photocatalysis is limited by its UV activation requirement because of its large band gap (3.2 or 3.0 eV in the anatase or rutile crystalline phase, respectively) [22]. Consequently, efforts have been channeled into shifting the optical sensitivity of  $\text{TiO}_2$  from UV to the visible-light region for the efficient utilization of solar energy, which is composed of only about 2–3% UV light. To extend the photo response of  $\text{TiO}_2$  to the visible region, many modification methods, such as metal ion doping [23], nonmetal doping [24], noble metal deposition [25,26], composite semiconductors [18,27], surface dye sensitization [28], and photosensitive material modification [29] have been reported [30]. Degussa P25 is an acclaimed  $\text{TiO}_2$  photocatalyst in the degradation of pollutants in aqueous media, but its band gap limits its operation to UV region. Previous studies [7,31] showed that doping  $\text{TiO}_2$  with some elements can enhance its photocatalytic potentialities. Therefore, the present work was designed to study the effect created by doping  $\text{TiO}_2$  with some elements to push its operation into the visible light region. A Ca–Ce–W–tri-doped  $\text{TiO}_2$  photocatalyst was developed for this purpose. The formulations and testing of its (Ca–Ce–W– $\text{TiO}_2$ ) performance on the visible light degradation of acid red 1 (AR1) are discussed.

## 2. Materials and methods

### 2.1. Preparation of the photocatalysts

The doped  $\text{TiO}_2$  was prepared by the sol–gel method using titanium (IV) butoxide ( $\text{Ti}(\text{OBu})_4$ ) (97% reagent grade obtained from SIGMA Aldrich Chemicals) as the precursor. The sol–gel method was chosen for the catalysts' preparation because of its advantages [7]. Solution A was prepared by dissolving appropriate amount of dopants (Ca, Ce, and W) in equal proportions of 99.9% ethanol and water which has  $\text{HNO}_3$  to enhance the hydrolysis of the  $\text{Ti}(\text{OBu})_4$ , while the

required amount of  $\text{Ti}(\text{OBu})_4$  was dissolved in ethanol (99.9% chromatography analysis grade, Merck, Germany) under stirring (solution B). Solution A was gradually poured into solution B and stirred for some time until sols were formed. The gel was obtained after aging the sols for 24 h at room temperature. The undoped (pure)  $\text{TiO}_2$  was prepared in the same way without addition of any dopant to solution A. The gel obtained after aging was dried at 70 °C in a Memmert oven until it was fully dried. About 0.2 g of the dry gel was taken into a Teflon-lined autoclave and 25 ml of ethanol and 2.5 ml distilled water were added. The content of the autoclave was then subjected to heat treatment at 200 °C for 8 h. At the end of the heat treatment, the sample was filtered and dried at 80 °C until it was fully dried. The dried sample was then stored in a sample bottle and kept in a desiccator for further use. The Ca–Ce–W– $\text{TiO}_2$  developed in this work will hereafter be referred to as composite catalyst.

The details of the preparation of the co-doped photocatalyst having the formula type  $\text{Ti}_{(1-x-y)}\text{Ca}_{(3x-y)}\text{Ce}_{(2x-y)}\text{W}_{(y/6)}\text{O}_{2(1-2(y-x))}$  (at  $y < 2x$  and  $x + y < 1$ ) are as follows: To prepare  $\text{I}_1$  (see Table 1) in a specific batch, 0.0283 g of calcium nitrate tetrahydrate, 0.0260 g cerium nitrate hexahydrate and 0.0290 g tungstophosphoric acid hydrate were dissolved in a solution of 0.514 mol ethanol mixed with equal volume of water, containing  $\text{HNO}_3$  to make solution A as described above, while 59.81 mmol titanium butoxide was dissolved in 0.686 mol of ethanol to make solution B. All other steps (the aging, drying, and hydrotreatment) followed thereafter are as described above.

### 2.2. Photocatalysts characterization

Nitrogen adsorption–desorption isotherms of the developed photocatalysts were collected on ASAP 2020 V3.02 H Micromeritics surface area and porosity analyzer at 77 K. The Brunauer–Emmett–Teller (BET) surface area was calculated from the linear part of the BET plot. The pore size distribution plots were obtained by using the Barret–Joyner–Halenda (BJH) model. Powder X-ray diffraction (XRD) patterns of the catalysts were measured by D8 Advanced X-Ray solution. The elemental compositions of the catalysts were determined using an energy dispersive X-ray detector mounted on a microscope. The microstructure and morphology of the prepared catalysts were observed using Philips XL30S model surface scanning electron microscopy (SSEM). The active surface functional groups present in the catalysts were determined by the Fourier transform infrared (FTIR). The spectra were recorded in the range of 4,000–400  $\text{cm}^{-1}$ . The X-ray photoelectron spectroscopy spectra (XPS) were

Table 1  
Formulations of the composite catalysts

Interactions (I)	Atomic compositions in the photocatalysts					Molecular formula
	Ti	Ca	Ce	W	O	
I <sub>1</sub>	0.9968	1.998E-3	9.99E-4	1.66E-4	1.9966	Ti <sub>0.9968</sub> Ca <sub>1.998E-3</sub> Ce <sub>9.99E-4</sub> W <sub>1.66E-4</sub> O <sub>1.9966</sub>
I <sub>2</sub>	0.9843	9.942E-3	4.97E-3	8.29E-4	1.9884	Ti <sub>0.9843</sub> Ca <sub>9.942E-3</sub> Ce <sub>4.97E-3</sub> W <sub>8.29E-4</sub> O <sub>1.9884</sub>
I <sub>3</sub>	0.9995	3.450E-4	1.50E-4	4.17E-5	1.9996	Ti <sub>0.9995</sub> Ca <sub>3.45E-4</sub> Ce <sub>1.5E-4</sub> W <sub>4.17E-5</sub> O <sub>1.9996</sub>
I <sub>4</sub>	0.9997	1.900E-4	9.00E-5	9.83E-5	2.0000	Ti <sub>0.9997</sub> Ca <sub>1.9E-4</sub> Ce <sub>9.0E-5</sub> W <sub>1.83E-5</sub> O <sub>2</sub>
I <sub>5</sub>	0.9998	1.199E-4	5.90E-5	1.02E-5	2.0000	Ti <sub>0.9998</sub> Ca <sub>1.199E-4</sub> Ce <sub>5.9E-5</sub> W <sub>1.02E-5</sub> O <sub>2</sub>
I <sub>6</sub>	0.9998	1.380E-4	6.80E-5	1.20E-5	1.9998	Ti <sub>0.9998</sub> Ca <sub>1.38E-4</sub> Ce <sub>6.8E-5</sub> W <sub>1.2E-5</sub> O <sub>1.9998</sub>
I <sub>7</sub>	0.9997	2.100E-4	1.00E-4	2.00E-5	1.9998	Ti <sub>0.9997</sub> Ca <sub>2.1E-4</sub> Ce <sub>1.0E-4</sub> W <sub>2.0E-5</sub> O <sub>1.9998</sub>

obtained with Mesin XPS Omicron els 5,000 spectrophotometer using Al K<sub>α</sub> at 1,480 kV as radiation X-ray source. All binding energies were calibrated to the C 1s peak at 284 eV. The UV–vis reflection spectra of the developed catalysts were measured using a Lamda 35 PerkinElmer UV–vis spectrophotometer.

### 2.3. Photocatalytic activities of the photocatalysts

The photocatalytic activities of the photocatalysts were performed in a 1-liter glass beaker. About 300 ml of the required concentration of AR1 was poured into the glass beaker and after the addition of 0.20 g of the photocatalyst to it; the sample which was equipped with a magnetic stirrer and an air pump to bubble air into it was exposed to visible light. The visible light was provided by a 150 W metal halide lamp source with a built-in cutoff filter (Model: Dolan-Jenner MH-100 Metal Halide Fiber Optic Illuminator) used to filter out the light of wavelengths below 400 nm. Samples were withdrawn from the irradiated solution at preset time intervals, filtered with 0.2-μm Whatman PTFE filter and analyzed for the concentration of the AR1 in the solution using a computer software attached to UV–vis Spectrophotometer, UV-1700 PharmaSpec, Shimadzu at 505 nm (maximum absorption wavelength of AR1). The degradation efficiency (percentage degradation) and the amount of pollutant removed were calculated by Eqs. (1) and (2), respectively:

$$\% \text{ degradation} = (C_0 - C_t)/C_0 \times 100 \quad (1)$$

$$\text{Amount of pollutant degraded} = C_0 - C_t \quad (2)$$

where C<sub>0</sub> and C<sub>t</sub> are the pollutant concentrations at time t=0 and time t.

To compare the activity of the developed photocatalysts, a commercially available TiO<sub>2</sub> photocatalyst, Degussa P25, was also employed in the visible light

photocatalytic degradation of AR1 using the same experimental conditions as in the case of the developed photocatalysts.

## 3. Results and discussion

### 3.1. Development of the photocatalyst

The literature [32] revealed that there was a better activity of composite photocatalysts than individually doped TiO<sub>2</sub> photocatalyst. As a result, an electronically stable TiO<sub>2</sub> photocatalyst, jointly doped with Ca, Ce, and W was developed having the formula type Ti<sub>(1-x-y)</sub>Ca<sub>(3x-y)</sub>Ce<sub>(2x-y)</sub>W<sub>(y/6)</sub>O<sub>2(1-2(y-x))</sub> (at y < 2x and x + y < 1). Different values of x and y within the specified limits were employed in the preparation of the composite photocatalysts. The activities of both the composite, individually doped or co-doped and undoped photocatalysts developed were tested in the visible light photocatalytic degradation of an azo dye, AR1. Using the above expression, the composite catalysts were formulated as shown in Table 1 and tested as described herewith. In preliminary experiments, the developed photocatalysts, I<sub>1</sub>–I<sub>4</sub> were tested under UV light irradiation as recorded in Section 3.3.

### 3.2. Characterization of photocatalysts

#### 3.2.1. Microstructure and morphology of the catalysts

The microstructure and morphology of the developed photocatalysts were studied using SEM. Fig. 1 shows the surface scanning electron micrograph of the crystals (a) Ca–Ce–W–doped TiO<sub>2</sub> composite photocatalyst, (b) Ca–Ce–doped TiO<sub>2</sub>, (c) Ce–W–doped TiO<sub>2</sub>, and (d) Ca–W–doped TiO<sub>2</sub>. Earlier results [31] revealed that the undoped TiO<sub>2</sub> sample treated in the same mode resulted in a dense crystalline surface material. A closer observation of the micrographs “a–d” revealed that the surfaces of all the photocatalysts had some sites occupied by the dopant(s). The

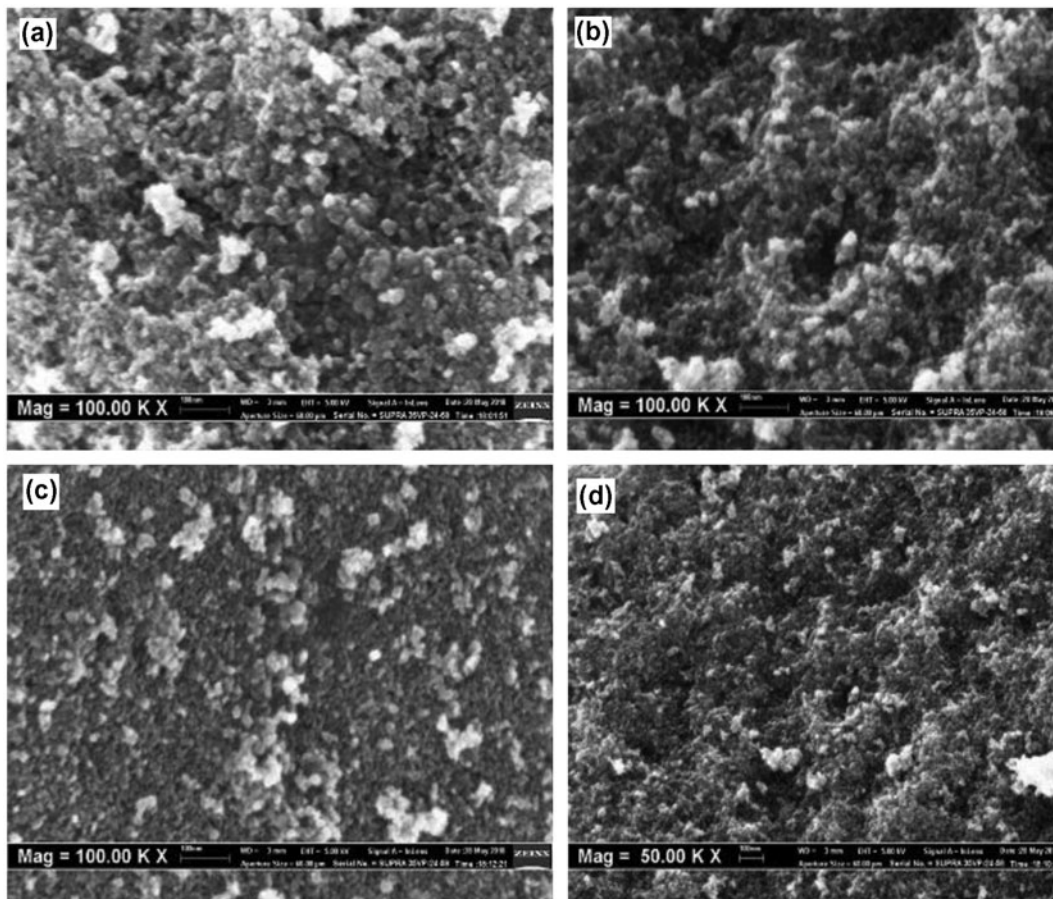


Fig. 1. SEM images of (a) composite photocatalyst,  $I_4$  [31] (b) Ca-Ce-TiO<sub>2</sub> on conditions of  $I_4$ , (c) Ce-W-TiO<sub>2</sub> on conditions of  $I_4$  and (d) Ca-W-TiO<sub>2</sub> on conditions of  $I_4$ .

portions which appeared stained are the sites occupied by the dopant(s). The results revealed that surfaces of photocatalysts are made up of a large number of aggregates of catalyst particles agglomerated together. The composite catalyst appeared to be the most stained, which means that most of the available vacancies on the surfaces were occupied by the dopants and were fully integrated together. The synergistic effects of the interactions of these dopants make the tri-doped sample more effective in photocatalytic activity than all others.

### 3.2.2. Structural and functional group analyses

The crystal phase compositions of the developed photocatalysts were determined by XRD measurements (using D8 Advanced X-ray solution). The results Fig. 2 show the XRD pattern of various crystals hydrotreated at 200°C for 8 h. The analysis of the photocatalysts as obtained from the XRD results is presented in Table 2. It is clear from the table that all

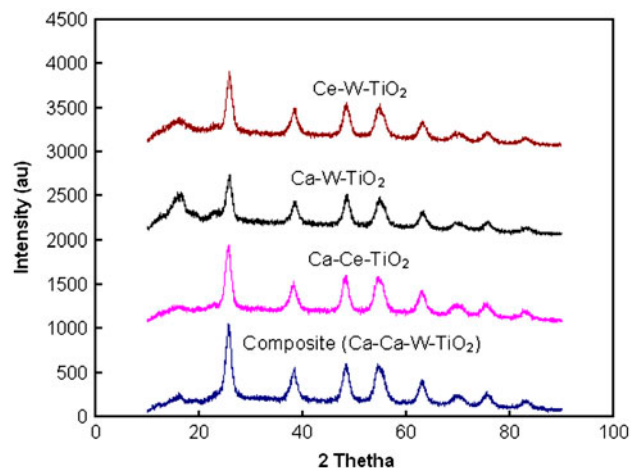


Fig. 2. XRD spectra of TiO<sub>2</sub>-based photocatalysts.

the catalysts, both composite and bi-doped, are of the same crystal phase (anatase) and have near-identical lattice parameters (crystals dimensions). All have

Table 2  
Hydrotreated photocatalysts crystals analysis

Sample	Crystal form	Structure	Lattice parameters (Å)			Crystal ID number	Wavelength (nm)	Cell volume (Å <sup>3</sup> )
			a	b	c			
Undoped TiO <sub>2</sub> *	Anatase	Tetragonal	3.7830	3.7830	9.4970	01-086-1157 (A)	1.5406	135.91
Ca–Ce–doped TiO <sub>2</sub>	Anatase	Tetragonal	3.7830	3.7830	9.5100	00-004-0477 (D)	1.5406	136.10
Ca–W–doped TiO <sub>2</sub>	Anatase	Tetragonal	3.7830	3.7830	9.4970	01-086-1157 (A)	1.5406	135.91
Ce–W–doped TiO <sub>2</sub>	Anatase	Tetragonal	3.7760	3.7760	9.4860	01-073-1764 (A)	1.5406	135.25
Composite catalyst*	Anatase	Tetragonal	3.7760	3.7760	9.4860	00-002-0406 (D)	1.5406	135.25

\*Akpan and Hameed [31].

tetragonal structures. In a previous study [31], it was noted that all doped samples have lattice parameters and cell volumes generally smaller than the undoped. The observation in the present study revealed that Ca–Ce–TiO<sub>2</sub> has a cell volume slightly larger than the undoped; Ca–W–TiO<sub>2</sub> has the same cell volume as the undoped, while both the composite and Ce–W–TiO<sub>2</sub> catalysts have cell volumes relatively smaller than the undoped. The increase or decrease in lattice parameters and cell volume imply that the doping introduced some levels of distortions in the crystal structure of the anatase TiO<sub>2</sub> and may likely affect the performance of the photocatalysts. Some inferences could be drawn from the intensities of the strongest anatase peaks at  $2\theta = 25.4^\circ$  (101). The results (Fig. 2) show that the most intense peak at this angle is the composite's, followed by Ca–Ce–TiO<sub>2</sub>, Ce–W–TiO<sub>2</sub>, and Ca–W–TiO<sub>2</sub> in descending order. Relating this to the visible light photocatalytic degradation of AR1 results (see Section 3.5), it is possible to claim that the effectiveness of each photocatalyst (within the limits of the experiment) is directly proportional to its intensity at the strongest anatase peak. The reason for the low activities of bi-doped catalysts may be closely related to the instability of these photocatalysts that were not developed to satisfy their electronic structure, but rather to satisfy the conditions laid down for the composite photocatalyst.

A close observation of the FTIR spectra (Fig. 3) revealed that there are some absorption bands in the regions of 440–541, 1,607, 3,722–3,763 in all the samples. There are also absorption bands in the region of 2,343 for three of the photocatalysts' samples, except for Ca–Ce–TiO<sub>2</sub>; at 2,323 for Ca–W–TiO<sub>2</sub> and Ce–W–TiO<sub>2</sub>, and at 1,040 for only Ca–W–TiO<sub>2</sub>. A little amount of absorption is noticed at the band of 1,394 for three of the samples except for the composite photocatalyst which appears to have a reflection at this band. Previous works [31,33,34] indicated that the absorption bands at the region of 3,300–3,500 and

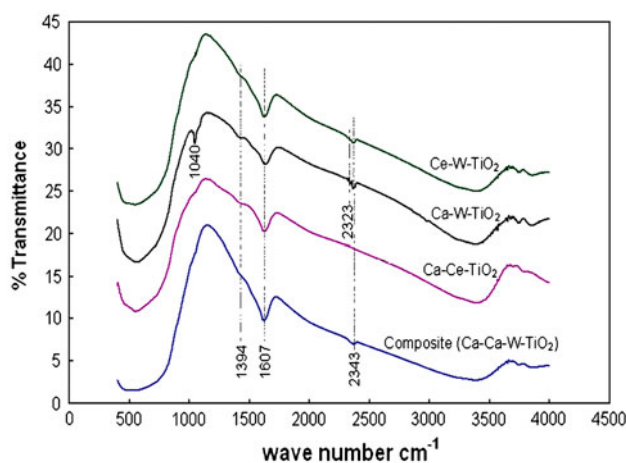


Fig. 3. FTIR spectra of TiO<sub>2</sub>-based photocatalysts.

1,636–1,634 cm<sup>-1</sup> are respectively, due to the stretching and bending vibrations of the hydroxyl on the surface of TiO<sub>2</sub> photocatalyst; therefore, the absorption band at about 3,400 and 1,607 cm<sup>-1</sup> can be assigned to the stretching and bending vibrations of the hydroxyl on the surface of the TiO<sub>2</sub> photocatalyst. The absorption band at the region of 440–541 cm<sup>-1</sup> is assigned to the stretching vibration of Ti–O. The absorption band at 3,763 cm<sup>-1</sup> may be attributed to the hydroxyl group chemisorbed on surface defected site or both the dissociation of water and molecularly adsorbed water [35]. The band at 1,040 cm<sup>-1</sup> on the Ca–W–TiO<sub>2</sub> may be attributed to C–O stretching. It is difficult to offer an explanation for this observation as all samples were prepared using the same precursor apart from the addition of the dopants. Nevertheless, it may be assumed that there existed some kinds of interaction between tungsten and carbon atoms present in the precursor, which could be responsible for the stretching, and as such affected the surface functional structure, which in turn affected the performance of the photocatalyst. The absorption bands at 2,323 and 2,343

are due to OH stretching. These noticeable differences at the band regions of  $1,040$ ,  $1,394$ , and  $2,323\text{ cm}^{-1}$  may account for the efficiency of the photocatalysts. The absorption band in the region of  $1,394\text{ cm}^{-1}$  is OH deformation; and this together with the C–O stretching absorption band in the region of  $1,040\text{ cm}^{-1}$  significantly reduced the activities of the affected photocatalysts. The large amount of OH groups present in the photocatalysts provided effective sites for photocatalysis, since it is a very good oxidant.

### 3.2.3. Surface area and pore size of the composite catalyst

Nitrogen adsorption–desorption isotherms of the developed photocatalysts were collected on ASAP 2020 V3.02 H Micromeritics surface area and porosity analyzer at 77 K to study the pore size distributions, surface area and the adsorption–desorption isotherm pattern of the photocatalysts. Fig. 4(i) is a representative of the nitrogen adsorption–desorption isotherm and the pore size distribution curve (inset) of all the photocatalysts developed in the present study. All the  $\text{TiO}_2$ -based photocatalysts developed during this investigation have similar nitrogen adsorption–desorption isotherms and pore size distribution curves. A distinguishing feature is observed in the  $\text{N}_2$  adsorption–desorption isotherms for all the hydrotreated photocatalysts; though, some little deviations are noticed with the Ce–W– $\text{TiO}_2$  photocatalysts that have an open loop (Fig. 4(ii)). At a relative pressure range from 0.45 to 1.0, all the hydrotreated photocatalysts exhibited  $\text{N}_2$  adsorption–desorption isotherms of type IV with type H2 hysteresis loops. The type H2 hysteresis loops represent the pore structure, size, and shape of materials which have disordered distributions, and these are a typical characteristic of mesoporous materials [36]. The BET surface area and pore size distributions of the photocatalysts are presented in Table 3. It can be seen from this table that the composite photocatalyst possesses the largest surface area, pore size, and pore volume which greatly enhance its visible light photocatalytic potentiality over others.

### 3.2.4. Chemical state analysis and UV–vis diffuse reflectance spectra

The chemical state of the elements which made up the building blocks for the composite photocatalyst has already been analyzed by XPS [31]. The results revealed that all the elements (Ca, Ce, W, and Ti) which participated in the development of the composite photocatalyst existed in their desired

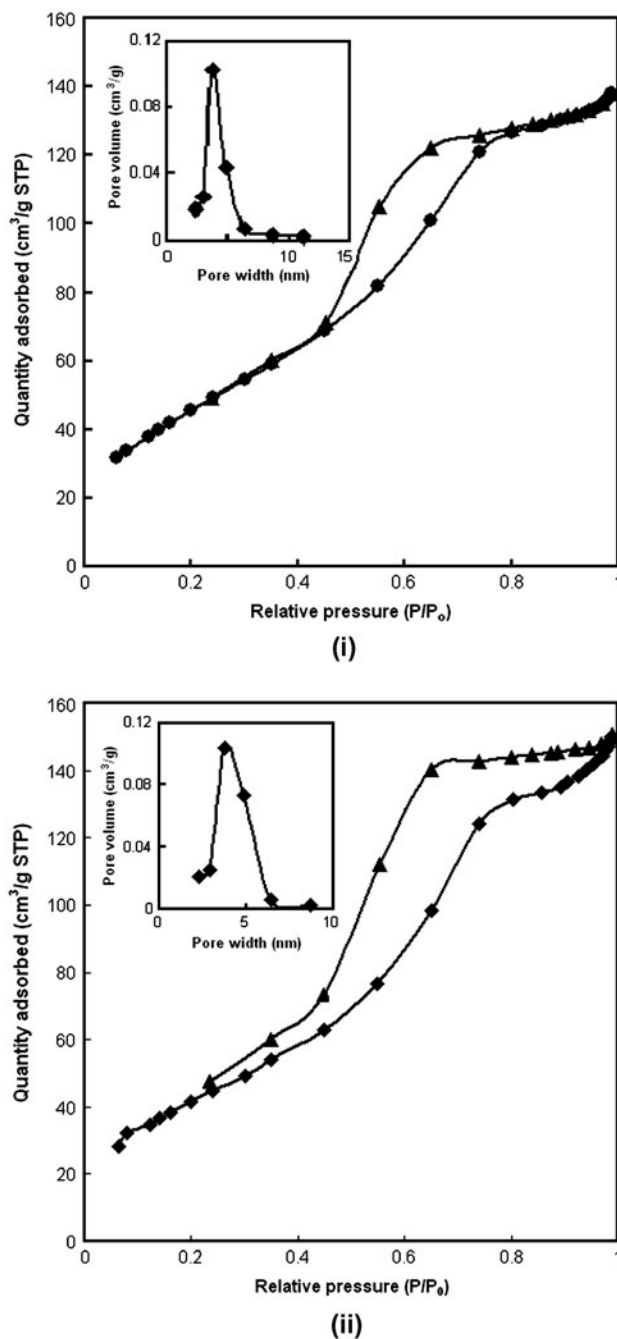


Fig. 4. Physisorption isotherms and pore size distributions inset for (i) Ca–W– $\text{TiO}_2$  and (ii) Ce–W– $\text{TiO}_2$  photocatalyst hydro treated at  $200^\circ\text{C}$  for 8 h.

oxidation states; hence, the composite photocatalyst is electronically stable.

The UV–vis analysis of the developed Ca–Ce–W-doped  $\text{TiO}_2$  composite photocatalyst showed that doping of  $\text{TiO}_2$  narrows its band gap by  $0.26\text{ eV}$  (from  $3.2\text{ eV}$  for anatase  $\text{TiO}_2$  to  $2.94\text{ eV}$  for the composite photocatalyst), while the undoped  $\text{TiO}_2$  has a shrink

Table 3  
BET surface area and pore size distributions data

Sample	BET surface area (m <sup>2</sup> /g)	BJH pore size (nm)	Pore volume (cm <sup>3</sup> /g)
Composite photocatalyst	209.53	5.120	0.2685
Ca–Ce–TiO <sub>2</sub> photocatalyst	187.88	4.190	0.2310
Ca–W–TiO <sub>2</sub> photocatalyst	175.68	4.227	0.2117
Ce–W–TiO <sub>2</sub> photocatalyst	158.37	4.906	0.2294

of 0.04 eV (from 3.2 to 3.16 eV). This will invariably push the activities of the composite photocatalyst more into visible region. Photon Energy,  $E_{\text{phot}}$  is related to the wave length,  $\lambda$  of the semiconductor photocatalyst as [37]:

$$E_{\text{phot}} = \frac{1239}{\lambda} \quad (3)$$

When the  $E_{\text{phot}}$  becomes the band gap energy of the semiconductor, the onset optical wavelength can be calculated from Eq. (3). In the present investigation, the onset optical wavelength for the pure TiO<sub>2</sub> and composite photocatalysts are 392.09 and 421.43 nm, respectively.

### 3.3. Photocatalytic degradation of dyes by UV light irradiation using the hydrotreated photocatalyst

Photocatalytic degradation of AR1 dye using UV light irradiation was first initiated to study the activity of the developed photocatalysts. The test was carried out for photocatalysts' interactions (I<sub>1</sub>–I<sub>4</sub>). Initially, two modes of heat treatment (calcination and hydrothermal) of the photocatalysts were adopted, and the photocatalysts' activities tested by the degradation of AR1. The results of the photocatalytic activities of the photocatalysts are shown in Fig. 5. Two of the samples I<sub>1</sub> and I<sub>2</sub> together with the undoped or pure TiO<sub>2</sub> were calcined at 450 °C for 3 h and their activities tested. It can be seen from the figure that I<sub>1</sub> and I<sub>2</sub> calcined at 450 °C for 3 h showed the least effectiveness in the degradation of AR1. The result here is not surprising as the formulation of I<sub>2</sub> was done in such a way that 3% by weight of Ca was present in it. It has already been established in a previous work [7] that beyond 1% by weight of Ca in TiO<sub>2</sub>, doping becomes detrimental to the activity of TiO<sub>2</sub>. The pure TiO<sub>2</sub> calcined at the same temperature performed better than both I<sub>1</sub> and I<sub>2</sub>. I<sub>2</sub> became worst as the amount of dye degraded in 240 min UV light irradiation was just 2.155 mg/l (about 9.06%) out of 23.775 mg/l as against 23.050 mg/l (about 96.95%) degraded by the pure TiO<sub>2</sub> at the same irradiation time. On the other hand,

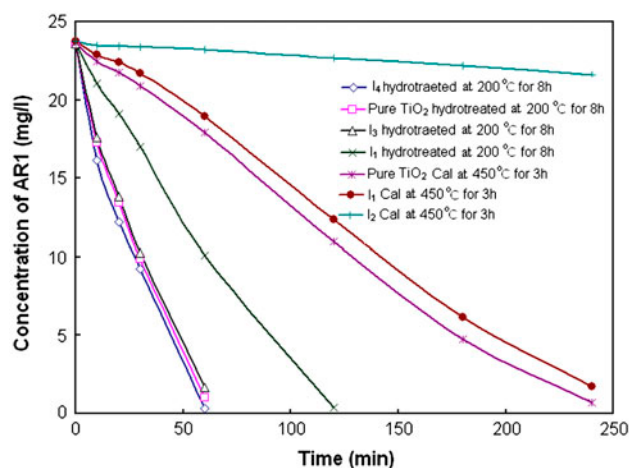


Fig. 5. Selection of the best photocatalyst for the degradation of AR1.

92.77% degradation was achieved by I<sub>1</sub> calcined at the same temperature for the same irradiation time. So I<sub>2</sub> was not further considered for hydrotreatment. Hence, the pure TiO<sub>2</sub>, I<sub>1</sub>, I<sub>3</sub>, and I<sub>4</sub> were subjected to hydrothermal treatment and the results showed that I<sub>4</sub> (the composite TiO<sub>2</sub> photocatalyst) became the best photocatalyst as there was almost a complete degradation (98.64%) in 60 min irradiation time. The pure hydrotreated TiO<sub>2</sub> had 95.69% degradation, while I<sub>3</sub> and I<sub>1</sub> hydrotreated catalysts had 93.02% and 57.43% degradation, respectively, at the same 60 min irradiation time. Though, the composite catalyst showed a slightly better performance in comparison with others when exposed to UV light irradiation, its performance was better in the visible region as it had earlier been demonstrated that its onset optical wavelength is in the visible range. The composite catalyst (I<sub>4</sub>) was then used to study its degradation efficiency on the AR1 visible light irradiation.

### 3.4. Photocatalytic degradation of AR1 under visible light

Fig. 6 shows a comparison between the catalysts developed according to the formulations shown in Table 1 (Formulations of the composite photocatalysts).

The initial test conducted on the formulated photocatalysts showed that  $I_1$  and  $I_2$  were totally unsuitable candidates for the photocatalytic process as a great deviation from  $I_4$  was noticed for them. As a result of this, they were not considered in the visible light experiment. Fig. 6 reveals that  $I_4$  was still superior in its photocatalytic ability to all other formulations, as there was 90.7% degradation of AR1 under visible light irradiation as against 59.7%, 57.4%, 54.6%, and 42.9% for  $I_7$ ,  $I_3$ ,  $I_6$ , and  $I_5$ , respectively, in 8-h irradiation. To be doubly certain that it was the synergetic effects of these combinations that gave it an advantage over the others, it was quite necessary to prepare individually and combinations of two element(s) doping under the same formulations as  $I_4$ . The results, Fig. 7, show that doping  $TiO_2$  by either one or a combination of two of the elements (considered in this study) in the same proportions with  $I_4$  reduces its photocatalytic potentiality in the visible light experiment, except for the case of Ca-doped- $TiO_2$  where the photocatalytic performance was quite similar to the undoped  $TiO_2$ . It has earlier been reported that doping  $TiO_2$  with some transition metals could be detrimental to the photocatalytic activity of  $TiO_2$  as a result of high electron density about the nucleus, which results in repulsion of any further electrons trying to come into it [21,38]. Therefore, the results obtained here are in no wise surprising. Calcium as element number 20 has a lesser concentration of electrons about its nucleus and might have allowed for interchange of electrons, hence its performance is closely similar to the undoped  $TiO_2$  in the visible light region.

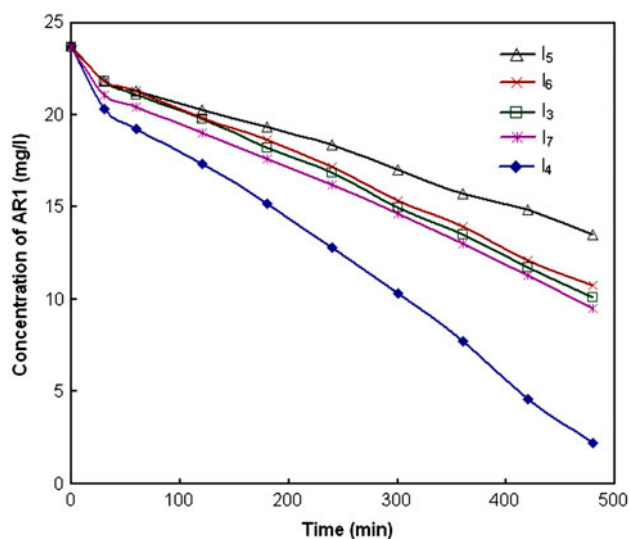


Fig. 6. Comparison of formulations (all hydrotreated at 200°C for 8 h) for visible light photocatalytic degradation of AR1.

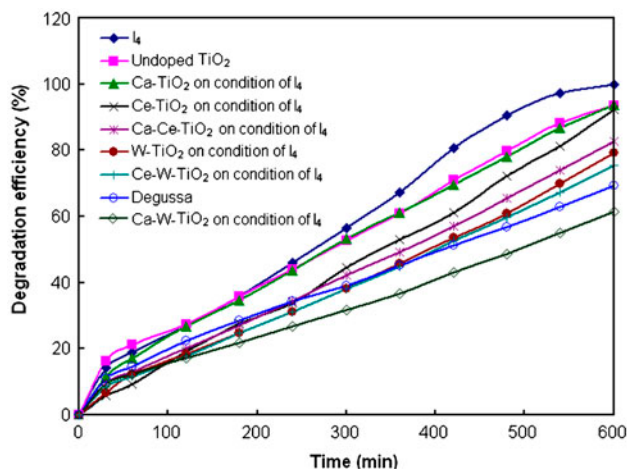


Fig. 7. Visible light photocatalytic degradation of AR1 using various photocatalysts developed on the same conditions of  $I_4$ .

Cerium is considered as luminescent element [39] and tends to push the photocatalytic activity of  $TiO_2$  toward the visible light region. Nevertheless, its high electron density towards the nucleus must have shielded it, preventing other electrons from entering into it, and hence, it has lower than expected level of activity, though, some level of increase are noticed. Tungsten has the highest concentration of electrons about its nucleus and its large size could not allow it to completely integrate into the lattices of  $TiO_2$ , and hence, it acts to reduce the photocatalytic activity of  $TiO_2$ . The interactions between only  $TiO_2$ , W, and Ca produced the worst visible light photocatalyst developed in this study. This can be attributed to electronic instability which might have set in at this point since the sample compositions which were used here were originally designed for  $I_4$ . It therefore applies that any instability in the electronic structure of the photocatalyst will also greatly influence its photocatalytic activities. Generally, apart from Ca-W-doped  $TiO_2$ , all other doped  $TiO_2$  considered in this study; in whatever arrangement are better in their visible light photocatalytic degradation performance than Degussa P25.

### 3.5. Visible light photocatalytic degradation of AR1 by $I_4$ in comparison with Degussa P25 and the undoped $TiO_2$

Subsequent to the establishment of the fact that  $I_4$  turned out to be the best photocatalysts developed in this study, a comparative study was then carried out to evaluate its performance in relations to both the undoped  $TiO_2$  and Degussa P25. About 100% degradation of AR1 was attained in 600 min (10 h) irradiation with visible light using  $I_4$  photocatalyst (Fig. 8). When the same photocatalytic operation was

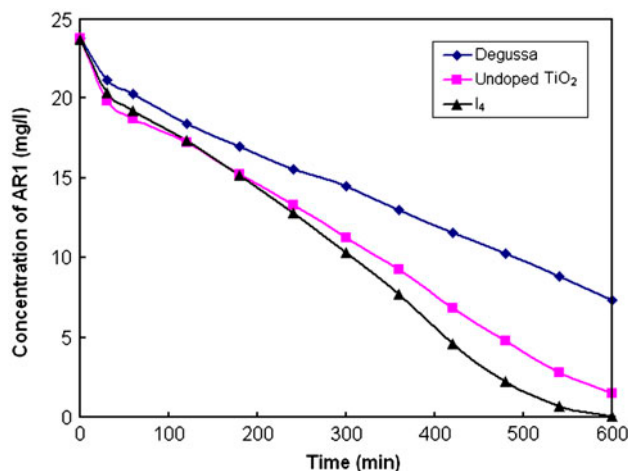


Fig. 8. Comparison between the developed catalysts and Degussa P25 under visible light irradiation.

undertaken by Degussa P25, only 69.1% degradation was achieved at the same irradiation time, while 92.8% degradation was achieved by the undoped TiO<sub>2</sub>. Earlier work [32] showed that Degussa P25 attained about 54% degradation in 7-h visible light irradiation of active yellow XRG dye, whereas all the samples doped with Cr<sup>3+</sup> from 0.05% to 0.2% were all better than the Degussa P25 in the visible light experiment. Sun et al. [40] on the other hand showed a much reduced amount of degradation of orange G (OG) in 150 min by Degussa P25. In both instances, a smaller percentage degradation by the undoped TiO<sub>2</sub> than by Degussa P25 was reported. The results of the present study are in perfect agreement with the fact that smaller quantity of the dye was degraded by Degussa P25 in 10 h visible light irradiation, but varied from their results in that the prepared undoped TiO<sub>2</sub> performed better than the Degussa P25 in visible light photocatalysis. These variations may be attributed to the methods and precursors used in the preparation of the catalysts, and subsequent heat treatment procedures.

### 3.6. Other operational parameters for the visible light photocatalysis of AR1 by I<sub>4</sub> catalysts

It has already been established in the literature [41] that operational parameters do affect the performance of any photocatalysts. Therefore, there was the need to investigate operational parameters influence on the visible light photocatalytic degradation of AR1. Hence, the effects of initial concentrations, initial pH of dye solutions and the hydrotreatment temperature of the catalyst on the visible light photocatalytic degradation of AR1 were investigated. The results (Fig. 9) present the effects of initial concentration of dye

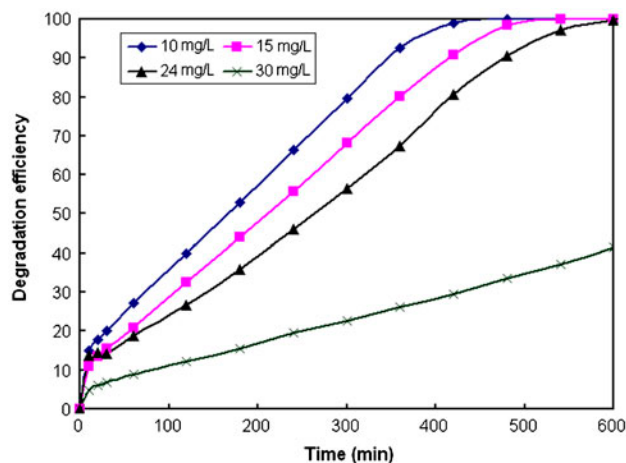


Fig. 9. Degradation efficiency of AR1 by I<sub>4</sub> photocatalyst on visible light photocatalysis at different initial concentrations of AR1.

solution on the visible light photocatalytic degradation of AR1 by I<sub>4</sub> photocatalyst. The reaction was greatly favored at lower initial concentrations as 100% degradation of AR1 was achieved at 480 min and 540 min visible light irradiation for 10 mg/l and 15 mg/l initial dye concentrations, respectively. 99.8% degradation of AR1 was also attained at 600 min visible light irradiation of 24 mg/l initial AR1 concentration. The visible light photocatalytic degradation of AR1 with I<sub>4</sub> as a photocatalyst became more difficult at higher initial dye concentrations. This trend of observations may not be unconnected with the color intensity of the dye which increases with the increase in concentration of the dye and hence the depth of penetration of light into the solution reduced with increase in concentration. This reduction in the depth of light penetration will (i) reduce the photon energy reaching the dye solution and (ii) shield the photocatalyst from the photon energy; and the end, result is a reduction in the activity of the photocatalyst. At 30 mg/l AR1 initial concentration, only 41.5% degradation (corresponding to 12.45 mg/l AR1 removal) was achieved at 600 min irradiation, whereas about 100% degradation was attained at 24 mg/l initial dye concentration. This shows that just about half of the concentration removed at lower initial concentration of 24 mg/l AR1 could be achieved at 30 mg/l initial concentration considering the same irradiation time. An attempt was also made to undertake the degradation of dye of 50 mg/l initial concentration. Only 4.7% degradation was achieved at 180 min visible light irradiation as against 15.5%, 35.9%, 44.1%, and 52.8% attained at 30 mg/l, 24 mg/l, 15 mg/l, and 10 mg/l initial concentrations, respectively. It was discovered that light penetration into the solutions became difficult

and hence impaired the photocatalytic reaction at higher initial concentrations. It must be noted here that light penetration into the solution depends on the photon energy available and this is directly dependent on the light intensity.

It was necessary at this point to evaluate the order of reaction, and initial rate expression, Eq. (4) was used for the evaluations.

$$-r_{A0} = kC_{A0}^n \quad (4)$$

Eq. (4) is transformed into a linear equation by taking the natural logarithm of both sides to yield Eq. (5).

$$\ln(-r_{A0}) = \ln k + n \ln C_{A0} \quad (5)$$

The initial rate plot for the visible light photocatalytic degradation of RO16 is shown in Fig. 10.

The slope of the plot which is the order of reaction ( $n$ ) is  $-0.5898$ . Since the order of reaction cannot be negative, this value implied that the reaction tends to zeroth order. This prompted further investigations into the order of the reaction. This was undertaken by plotting the integrated forms of the zero, first, second, and third orders of reaction using the data obtained with 10–30 mg/l initial dye concentrations in the visible light photocatalytic degradation of AR1 (figures not shown). The degree of fitness of each order was evaluated by determining the values of  $R^2$ , and the

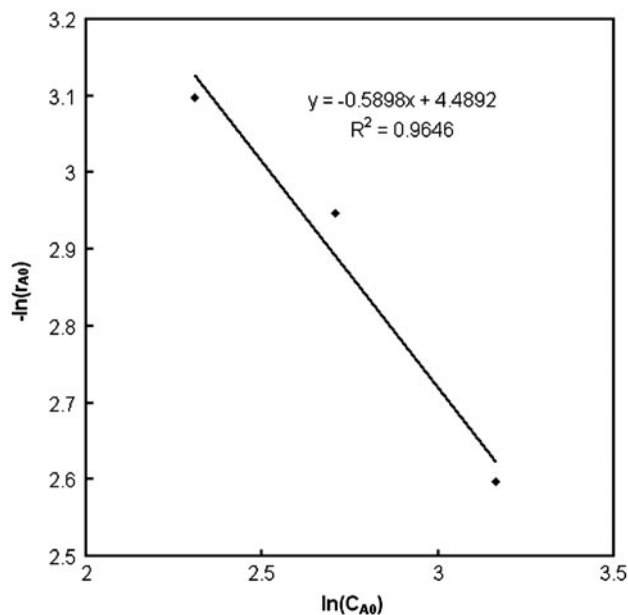


Fig. 10. Initial rate plot for the visible light photocatalytic degradation of AR1.

results are presented in Table 4. The  $R^2$  values for zero-order reaction rate ranges from 0.9326 to 0.9671, first-order reaction rate ranges from 0.7221 to 0.9755, second-order reaction rate ranges from 0.2850 to 0.9805 and third-order reaction rate ranges from 0.4531 to 0.9591. The outcome of these results shows that the reaction is independent of the initial concentrations of the dye. That means that the zero-order reaction model best describes the visible light photocatalytic degradation of AR1 using the  $I_4$  (composite) photocatalyst. Since the reaction is zero order, the effects of hydrotreatment temperature and time were appraised by their rates.

Fig. 11 shows the effects of hydrotreatment temperature on the rate of degradation of AR1 under visible light irradiation. It can be seen from the figure that the rate of degradation of AR1 increases almost proportionately as the temperature increased from 140 to 180°C, the magnitude of the increase in temperature from 180 to 200°C tend to reduce. This indicates that there must be an optimum temperature where a further increment in temperature will not further enhance the degradation rate. Testing temperature higher than 200°C was limited by the thermal regulator system which is designed to have a maximum operating temperature of 200°C. Nevertheless, from the plot of Fig. 11 it is clear that there is a shift in linearity between the hydrotreatment temperature of 180 and 200°C, tending to reach a plateau.

Fig. 12 shows the effect of initial pH of dye solution on the visible light photocatalytic degradation of AR1 using  $I_4$  photocatalyst. Within 10 min irradiation of the solution of initial pH 3, almost 100% color removal was achieved. It is important to state that though there was color removal, degradation definitely did not take place as the color removal was predominated by adsorption. The dye was vividly seen on the surfaces of the photocatalyst while the solution appeared to be clear. This was the observation for the first 10–240 min, but with continued irradiation, there was a gradual degradation. At the unadjusted dye pH of 5.75, 67.3% degradation was attained at 360 min irradiation. At higher pH, the visible light photocatalytic degradation of AR1 dye became difficult. The explanation for this is related to the point of zero charge of the photocatalyst which is already elaborated elsewhere [7]. At a neutral pH (7), only 10.6% (2.317 mg/l removal) AR1 degradation was achieved at 360 min irradiation. At pH 10, a negative development was recorded. There was an initial drop in concentration of the dye from 23.671 to 22.195 mg/l indicating initial color removal of 6.2%. But after this initial color removal, the dye concentration gradually increased to 24.7 mg/l (1.029 mg/l) above the dye concentration at the onset

Table 4  
Determination of the reaction rate order with corresponding constant which best fit the data for different initial concentrations of AR1 under visible light irradiation

Reaction order	Initial concentration of AR1 (mg/L)			
	10	15	24	30
Zero {mg/(L)(min)}	0.0260	0.9326	0.9671	15.000
First (L/min)	0.0075	0.8208	0.8134	0
Second L/(mg)(min)}	0.0118	0.4272	0.4155	-0.3038
Third L <sup>2</sup> /(mg)(min)}	0.0006	0.7301	0.6862	-0.0050
	$k_{app}$	$k_{app}$	$k_{app}$	$k_{app}$
	0.033	0.0059	0.0045	0.0002
	$R^2$	0.9671	0.8134	0.9671
	$C^*$	10.000	0	15.000
	$R^2$	0.9326	0.8208	0.8134
	$C^*$	0	0.7441	0
	$R^2$	0.4272	0.4155	0.4155
	$C^*$	-0.0092	-0.0002	-0.0050
	$R^2$	0.7301	0.6862	0.6862
	$C^*$	0	0	0
	$R^2$	0.9638	0.7221	0.7221
	$C^*$	23.678	0	23.678
	$R^2$	0.2850	0.2850	0.2850
	$C^*$	-0.0166	-0.0166	-0.0166
	$R^2$	0.9521	0.9521	0.9521
	$C^*$	0	0	0
	$R^2$	0.9805	0.9805	0.9805
	$C^*$	-0.0011	-0.0011	-0.0011

\*C is the point of intercept on the ordinate.

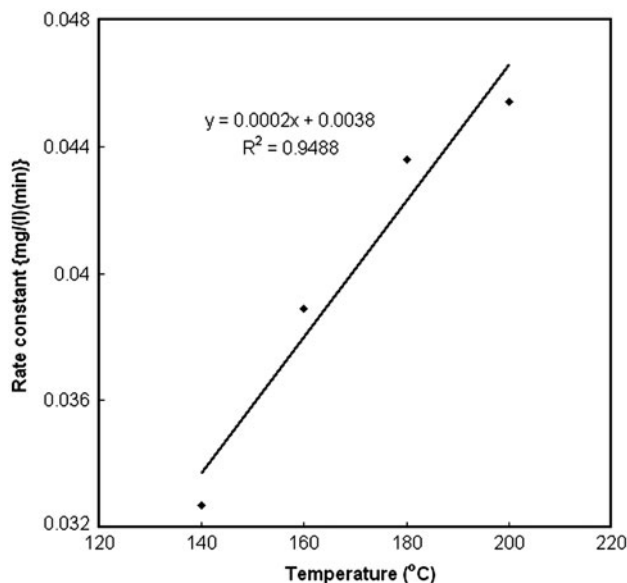


Fig. 11. Effects of hydrotreatment temperature on the rate constant for the visible light degradation of AR1.

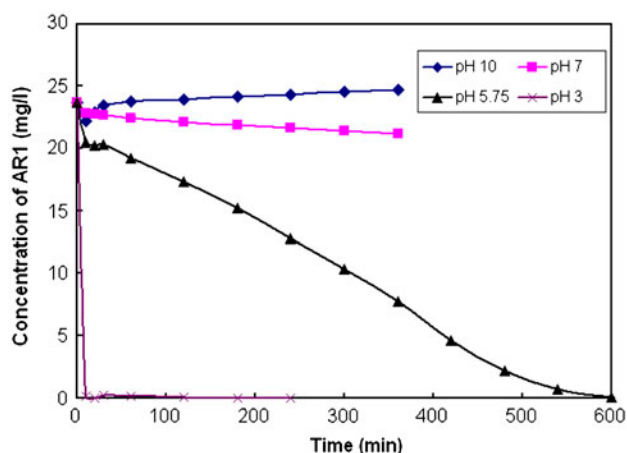


Fig. 12. Effect of initial pH of AR1 on its visible light photocatalytic degradation using I<sub>4</sub> photocatalyst.

of the experiment at 360 min visible light irradiation. It is assumed that at a particular pH, the dye and the photocatalyst must have formed a complex as a result of the irradiation by the visible light, and the new complex increase the absorptivity of the dye beyond its original absorptivity.

### 3. Conclusion

A Ca-Ce-W-doped-TiO<sub>2</sub> photocatalyst was successfully developed and tested in the visible light degradation of AR1. Various combinations were developed and tested. The visible light photocatalysis

is concentration-dependent. High initial concentrations of AR1 dye preclude the photon energy from reaching the photocatalyst and hence reduced its degradation rate. This was clearly demonstrated at 30 mg/l initial AR1 dye concentration where only 12.45 mg/l of dye was degraded (about half of the amount degraded at the same 600 min visible light irradiation time when 24 mg/l initial concentration was used). In comparison with Degussa P25, the developed tri-doped-TiO<sub>2</sub> is excellent in the visible light photocatalytic degradation of AR1 as about 99.8% degradation was achieved with it as against 69.2% degradation with Degussa P25 at 600 min irradiation under the same experimental conditions. The initial pH of dye solution exerts severe influence on the visible light degradation of the dye. At high initial solution pH 10, the visible light photocatalytic reaction was negatively affected as there appeared to be formation of complexes leading to the increase in absorptivity of the dye beyond its original absorptivity. At lower pH 3, the process is controlled by adsorption and hence may not be termed photocatalysis at such a condition.

The properties of the developed composite photocatalyst are responsible for its excellent performance. Doping TiO<sub>2</sub> with Ca, Ce, and W in the proposed proportions effected a red shift in its band gap from 3.2 to 2.94 eV resulting in the shift of the onset optical wavelength from 387.19 to 421.43 nm. It has a large surface area (209.53 m<sup>2</sup>/g), pore size (5.120 nm), and pore volume (0.2685 cm<sup>3</sup>/g) which greatly enhanced its photocatalytic activity. The photocatalytic effectiveness of each photocatalyst prepared is proportional to its intensity at the strongest anatase peak (101) at  $2\theta = 25.4^\circ$ , and the tri-doped TiO<sub>2</sub> has more intense peak than others at this angle.

### Acknowledgment

The authors acknowledge the research grant provided by Universiti Sains Malaysia under the RU Grant Scheme (RU Grant No.: 814005) which significantly sustained these investigations.

### References

- [1] S. Aber, M. Sheydaei, Application of physicochemically prepared activated carbon fiber for the removal of basic blue 3 from water, *Desalin. Water Treat.* 28 (2011) 97–102.
- [2] B.H. Hameed, I.A.W. Tan, Nitric acid-treated bamboo waste as low-cost adsorbent for removal of cationic dye from aqueous solution, *Desalin. Water Treat.* 21 (2010) 357–363.
- [3] R.B.M. Bergaminia, E.B. Azevedob, L.R.R.d. Araujo, Heterogeneous photocatalytic degradation of reactive dyes in aqueous TiO<sub>2</sub> suspensions: Decolorization kinetics, *Chem. Eng. J.* 149 (2009) 215–220.
- [4] N.K. Daud, U.G. Akpan, B.H. Hameed, Decolorization of sunzol black DN conc. in aqueous solution by Fenton oxidation process, effect of system parameters and kinetic study, *Desalin. Water Treat.* 37 (2012) 1–7.
- [5] U.G. Akpan, B.H. Hameed, Photocatalytic degradation of 2, 4-dichlorophenoxyacetic acid by Ca–Ce–W–TiO<sub>2</sub> composite photocatalyst, *Chem. Eng. J.* 173 (2011) 369–375.
- [6] G. McKay, M. Hadi, M.T. Samadi, A.R. Rahmani, M.S. Aminabad, F. Nazemi, Adsorption of reactive dye from aqueous solutions by compost, *Desalin. Water Treat.* 28 (2011) 164–173.
- [7] U.G. Akpan, B.H. Hameed, Enhancement of photocatalytic activity of TiO<sub>2</sub> by doping it with calcium ions, *J. Colloid Interface Sci.* 157 (2011) 168–178.
- [8] C. Li, N.-Y. Gao, W. Li, Photochemical degradation of typical herbicides simazine by UV/H<sub>2</sub>O<sub>2</sub> in aqueous solution, *Desalin. Water Treat.* 36 (2011) 197–202.
- [9] Q. Chen, W. Shi, Y. Xu, D. Wu, Y. Sun, Visible-light-responsive Ag–Si codoped anatase TiO<sub>2</sub> photocatalyst with enhanced thermal stability, *Mater. Chem. Phys.* 125(3) (2011) 825–832.
- [10] Z. Barhon, F. Bozon-Verduraz, N. Saffaj, A. Albizane, M. Azzi, M. Kacimi, M. Ziyad, Photodegradation of indigo carmine in aqueous solution by zirconium phosphates, *Desalin. Water Treat.* 30 (2011) 69–73.
- [11] M.H. Habibi, I.A. Farsani, Enhanced photocatalytic degradation of C.I. Reactive Orange 86 in aqueous environment using nanostructure Zn<sub>1-x</sub>Co<sub>x</sub>O composite thin film coated on glass, *Desalin. Water Treat.* 22 (2010) 204–210.
- [12] M. Shao, J. Han, M. Wei, D.G. Evans, X. Duan, The synthesis of hierarchical Zn–Ti layered double hydroxide for efficient visible-light photocatalysis, *Chem. Eng. J.* 168(2) (2011) 519–524.
- [13] X. Li, B. Yue, J. Ye, Photocatalytic hydrogen evolution over SiO<sub>2</sub>-pillared and nitrogen-doped titanate under visible light irradiation, *Appl. Catal. A* 390(1–2) (2010) 195–200.
- [14] O.A. Salu, M. Adams, P.K.J. Robertson, L.S. Wong, C. McCullagh, Remediation of oily wastewater from an interceptor tank using a novel photocatalytic drum reactor, *Desalin. Water Treat.* 26 (2011) 87–91.
- [15] G. Kenanakis, N. Katsarakis, Light-induced photocatalytic degradation of stearic acid by *c*-axis oriented ZnO nanowires, *Appl. Catal. A* 378(2) (2010) 227–233.
- [16] B.H. Hameed, U.G. Akpan, K.P. Wee, Photocatalytic degradation of Acid Red 1 dye using ZnO catalyst in the presence and absence of silver, *Desalin. Water Treat.* 27 (2011) 204–209.
- [17] M. Zhang, T. An, X. Hu, C. Wang, G. Sheng, J. Fu, Preparation and photocatalytic properties of a nanometer ZnO–SnO<sub>2</sub> coupled oxide, *Appl. Catal. A* 260(2) (2004) 215–222.
- [18] K.H. Hu, Z. Liu, F. Huang, X.G. Hu, C.L. Han, Synthesis and photocatalytic properties of nano-MoS<sub>2</sub>/kaolin composite, *Chem. Eng. J.* 162 (2010) 836–843.
- [19] C. Shifu, Z. Wei, Z. Sujuan, L. Wei, Preparation, characterization and photocatalytic activity of N-containing ZnO powder, *Chem. Eng. J.* 148 (2009) 263–269.
- [20] H. Xu, H. Li, G. Sun, J. Xia, C. Wu, Z. Ye, Q. Zhang, Photocatalytic activity of La<sub>2</sub>O<sub>3</sub>-modified silver vanadates catalyst for Rhodamine B dye degradation under visible light irradiation, *Chem. Eng. J.* 160 (2010) 33–41.
- [21] U.G. Akpan, B.H. Hameed, The advancements in sol–gel method of doped-TiO<sub>2</sub> photocatalysts, *Appl. Catal. A* 375 (2010) 1–11.
- [22] X. Yang, C. Cao, L. Erickson, K. Hohn, R. Maghirang, K. Klabunde, Photo-catalytic degradation of Rhodamine B on C-, S-, N-, and Fe-doped TiO<sub>2</sub> under visible-light irradiation, *Appl. Catal. B* 91 (2009) 657–662.
- [23] T.Z. Tong, J.L. Zhang, B.Z. Tian, F. Chen, D.N. He, Preparation of Fe<sup>3+</sup>-doped TiO<sub>2</sub> catalysts by controlled hydrolysis of titanium alkoxide and study on their photocatalytic activity for methyl orange degradation, *J. Hazard. Mater.* 155 (2008) 572–579.
- [24] G. Liu, X. Wang, Z. Chen, H.-M. Cheng, G.Q. (Max) Lu, The role of crystal phase in determining photocatalytic activity of nitrogen doped TiO<sub>2</sub>, *J. Colloid Interface Sci.* 329 (2009) 331–338.

- [25] Y. Ishibai, J. Sato, T. Nishikawa, S. Miyagishi, Synthesis of visible-light active TiO<sub>2</sub> photocatalyst with Pt-modification: Role of TiO<sub>2</sub> substrate for high photocatalytic activity, *Appl. Catal. B* 79 (2008) 117–121.
- [26] Z.L. Jin, X.J. Zhang, G.X. Lu, S.B. Li, Improved quantum yield for photocatalytic hydrogen generation under visible light irradiation over eosin sensitized TiO<sub>2</sub>-investigation of different noble metal loading, *J. Mol. Catal. A: Chem.* 259 (2006) 275–280.
- [27] Y.H. Xu, Z.X. Zeng, The preparation, characterization, and photocatalytic activities of Ce-TiO<sub>2</sub>/SiO<sub>2</sub>, *J. Mol. Catal. A: Chem.* 279 (2008) 77–81.
- [28] K.S. Yao, D.Y. Wang, C.Y. Chang, K.W. Weng, L.Y. Yang, S.J. Lee, T.C. Cheng, C.C. Hwang, Photocatalytic disinfection of phytopathogenic bacteria by dye-sensitized TiO<sub>2</sub> thin film activated by visible light, *Surf. Coat. Technol.* 202 (2007) 1329–1332.
- [29] Y.J. Zang, R. Farnood, Photocatalytic activity of AgBr/TiO<sub>2</sub> in water under simulated sunlight irradiation, *Appl. Catal. B* 79 (2008) 334–340.
- [30] D. Wang, J. Zhang, Q. Luo, X. Li, Y. Duan, J. An, Characterization and photocatalytic activity of poly (3-hexylthiophene)-modified TiO<sub>2</sub> for degradation of methyl orange under visible light, *J. Hazard. Mater.* 169 (2009) 546–550.
- [31] U.G. Akpan, B.H. Hameed, Solar degradation of an azo dye, acid red 1, by Ca-Ce-W-TiO<sub>2</sub> composite catalyst, *Chem. Eng. J.* 169 (2011) 91–99.
- [32] J. Zhu, Z. Deng, F. Chen, J. Zhang, H. Chen, M. Anpo, J. Huang, L. Zhang, Hydrothermal doping method for preparation of Cr<sup>3+</sup>-TiO<sub>2</sub> photocatalysts with concentration gradient distribution of Cr<sup>3+</sup>, *Appl. Catal. B* 62 (2006) 329–335.
- [33] Y. Li, C. Xie, S. Peng, G. Lu, S. Li, Eosin Y-sensitized nitrogen-doped TiO<sub>2</sub> for efficient visible light photocatalytic hydrogen evolution, *J. Mol. Catal. A: Chem.* 282 (2008) 117–123.
- [34] S. Liu, X. Chen, X. Chen, Preparation of N-Doped visible-light response nanosize TiO<sub>2</sub> photocatalyst using the acid-catalyzed hydrolysis method, *Chin. J. Catal.* 27(8) (2006) 697–702.
- [35] M. Janus, J. Choina, A.W. Morawski, Azo dyes decomposition on new nitrogen-modified anatase TiO<sub>2</sub> with high adsorptivity, *J. Hazard. Mater.* 166 (2009) 1–5.
- [36] W. Ren, Z. Ai, F. Jia, L. Zhang, X. Fan, Z. Zou, Low temperature preparation and visible light photocatalytic activity of mesoporous carbon-doped crystalline TiO<sub>2</sub>, *Appl. Catal. B* 69 (2007) 138–144.
- [37] M.P. Reddy, A. Venugopal, M. Subrahmanyam, Hydroxyapatite photocatalytic degradation of calmagite (an azo dye) in aqueous suspension, *Appl. Catal. B* 69 (2007) 164–170.
- [38] J.C. Colmenares, M.A. Aramendia, A. Marinas, J.M. Marinas, F.J. Urbano, Synthesis, characterization and photocatalytic activity of different metal-doped titania systems, *Appl. Catal. A* 306 (2006) 120–127.
- [39] L.Q. Jing, X.J. Sun, W.M. Cai, X.Q. Li, H.G. Fu, H.G. Hou, Photoluminescence of Ce doped TiO<sub>2</sub> nanoparticles and their photocatalytic activity, *Acta Chim. Sinica* 8 (2003) 1241–1245.
- [40] J. Sun, L. Qiao, S. Sun, G. Wang, Photocatalytic degradation of Orange G on nitrogen-doped TiO<sub>2</sub> catalysts under visible light and sunlight irradiation, *J. Hazard. Mater.* 155 (2008) 312–319.
- [41] U.G. Akpan, B.H. Hameed, Parameters affecting the photocatalytic degradation of dyes using TiO<sub>2</sub>-based photocatalysts: A review, *J. Hazard. Mater.* 170 (2009) 520–529.